



HAL
open science

Hyperfine excitation of SH^+ by H

François Lique, Alexandre Zanchet, Niyazi Bulut, Javier R. Goicoechea,
Octavio Roncero

► **To cite this version:**

François Lique, Alexandre Zanchet, Niyazi Bulut, Javier R. Goicoechea, Octavio Roncero. Hyperfine excitation of SH^+ by H . *Astronomy and Astrophysics - A&A*, 2020, 638, pp.A72. 10.1051/0004-6361/202038041 . hal-02903849

HAL Id: hal-02903849

<https://hal.science/hal-02903849>

Submitted on 21 Jul 2020

HAL is a multi-disciplinary open access archive for the deposit and dissemination of scientific research documents, whether they are published or not. The documents may come from teaching and research institutions in France or abroad, or from public or private research centers.

L'archive ouverte pluridisciplinaire **HAL**, est destinée au dépôt et à la diffusion de documents scientifiques de niveau recherche, publiés ou non, émanant des établissements d'enseignement et de recherche français ou étrangers, des laboratoires publics ou privés.



Distributed under a Creative Commons Attribution 4.0 International License

Hyperfine excitation of SH⁺ by H

François Lique¹, Alexandre Zanchet^{2,3}, Niyazi Bulut⁴, Javier R. Goicoechea², and Octavio Roncero²

¹ LOMC – UMR 6294, CNRS-Université du Havre, 25 rue Philippe Lebon, BP 1123, 76 063 Le Havre cedex, France
e-mail: francois.lique@univ-lehavre.fr

² Instituto de Física Fundamental, CSIC, C/Serrano, 123, 28006 Madrid, Spain

³ Departamento de Química Física, Facultad de Ciencias Químicas, Universidad de Salamanca, 37008 Salamanca, Spain

⁴ Firat University, Department of Physics, 23169 Elazığ, Turkey

Received 27 March 2020 / Accepted 24 April 2020

ABSTRACT

Context. SH⁺ is a surprisingly widespread molecular ion in diffuse interstellar clouds. There, it plays an important role by triggering the sulfur chemistry. In addition, SH⁺ emission lines have been detected at the UV-illuminated edges of dense molecular clouds, so-called photo-dissociation regions (PDRs), and toward high-mass protostars. An accurate determination of the SH⁺ abundance and of the physical conditions prevailing in these energetic environments relies on knowing the rate coefficients of inelastic collisions between SH⁺ molecules and hydrogen atoms, hydrogen molecules, and electrons.

Aims. We derive SH⁺-H fine and hyperfine-resolved rate coefficients from recent quantum calculations for the SH⁺-H collisions, including inelastic, exchange, and reactive processes.

Methods. The method we used is based on the infinite-order sudden approach.

Results. State-to-state rate coefficients between the first 31 fine levels and 61 hyperfine levels of SH⁺ were obtained for temperatures ranging from 10 to 1000 K. Fine-structure resolved rate coefficients present a strong propensity rule in favor of $\Delta j = \Delta N$ transitions. The $\Delta j = \Delta F$ propensity rule is observed for the hyperfine transitions.

Conclusions. The new rate coefficients will help significantly in the interpretation of SH⁺ spectra from PDRs and UV-irradiated shocks where the abundance of hydrogen atoms with respect to hydrogen molecules can be significant.

Key words. molecular data – molecular processes – radiative transfer – methods: laboratory: molecular

1. Introduction

Submillimeter absorption lines from the ground-rotational state of SH⁺ were first detected toward the W3 IRS5 high-mass star-forming region with *Herschel*/HIFI (Benz et al. 2010). In parallel, and using the APEX telescope, Menten et al. (2011) detected rotational absorption lines produced by SH⁺ in the low-density ($n_{\text{H}} \lesssim 100 \text{ cm}^{-3}$) diffuse clouds in the line of sight toward the strong continuum source SgrB2(M) in the Galactic center. Despite the very endothermic formation route of this hydride ion (for a review, see Gerin et al. 2016), subsequent absorption measurements of multiple lines of sight with *Herschel* demonstrated the ubiquitous presence of SH⁺ in diffuse interstellar clouds (Godard et al. 2012).

SH⁺ rotational lines have also been detected in emission toward the Orion Bar photodissociation region (PDR; Nagy et al. 2013), a strongly UV-irradiated surface of the Orion molecular cloud (e.g., Goicoechea et al. 2016). In warm and dense PDRs ($n_{\text{H}} \gtrsim 10^5 \text{ cm}^{-3}$) such as the Orion Bar, SH⁺ forms by exothermic reactions of S⁺ with vibrationally excited H₂ (with $v \geq 2$, see details in Agúndez et al. 2010; Zanchet et al. 2013, 2019). High angular resolution images taken with ALMA show that SH⁺ arises from a narrow layer at the edge of the PDR, the photodissociation front that separates atomic from molecular gas (Goicoechea et al. 2017). In these PDR layers, the abundance of hydrogen atoms is comparable to that of hydrogen molecules, which are continuously being photodissociated. Both H and H₂, together with electrons (arising from the ionization of carbon atoms, see e.g., Cuadrado et al. 2019), drive the collisional excitation of molecular rotational levels and atomic fine-structure levels.

In addition to PDRs, the SH⁺ line emission observed toward massive protostars likely arises from the UV-irradiated cavities of their molecular outflows (Benz et al. 2010, 2016). In these UV-irradiated shocks, the density of hydrogen atoms can be high as well. All in all, the molecular abundances and physical conditions in these regions, where atomic and molecular hydrogen can have comparable abundances, are not well understood.

In the interstellar medium (ISM), molecular abundances are derived from excitation line modeling. Assuming local thermodynamic equilibrium (LTE) conditions in the interstellar media with low densities is generally not a good approximation, as discussed by Roueff & Lique (2013). Hence, the population of molecular levels is driven by the competition between collisional and radiative processes. It is then essential to determine accurate collisional data between the involved molecules and the most abundant interstellar species, which are usually electrons and atomic and molecular hydrogen, in order to obtain reliably modeled spectra.

The computation of collisional data for the SH⁺ started recently. First, *R*-matrix calculations combined with the adiabatic-nucleus rotation and Coulomb-Born approximations was used to compute electron-impact rotational rate coefficients, and hyperfine-resolved rate coefficients were deduced using the infinite-order sudden approximation (Hamilton et al. 2018). Then, time-independent close-coupling quantum-scattering calculations were employed by Dagdigian (2019) to compute hyperfine-resolved rate coefficients for (de-)excitation of SH⁺ in collisions with both para- and ortho-H₂.

Collisional data with atomic hydrogen are much more challenging to compute because of the possible reactive nature of the

SH⁺–H collisional system. However, we have recently overcome this difficult problem and presented quantum mechanical calculations of cross sections and rate coefficients for the rotational excitation of SH⁺ by H, including the reactive channels (Zanchet et al. 2019), using new accurate potential energy surfaces.

Unfortunately, it was not possible to include the fine and hyperfine structure of the SH⁺(³Σ⁻) molecule in the quantum dynamical calculations, but they are resolved in astronomical observations. This made the new set of data difficult to use in astrophysical applications.

The aim of this work is to use the quantum state-to-state rate coefficients for the SH⁺(³Σ⁻)–H inelastic collisions to generate a new set of fine and hyperfine resolved data that can be used in radiative transfer models. The paper is organized as follows: Sect. 2 provides a brief description of the theoretical approach. In Sect. 3 we present the results. Concluding remarks are presented in Sect. 4.

2. Computational method

2.1. Potential energy surfaces

The collisions between SH⁺(X³Σ⁻) and H(²S) can take place on two different potential energy surfaces (PESs), the ground quartet (⁴A'') and doublet (²A'') electronic states of the H₂S⁺ system. In this work, we use the H₂S⁺ quartet and doublet PESs that were previously generated by Zanchet et al. (2019).

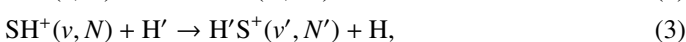
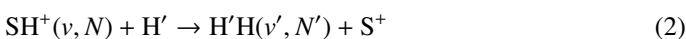
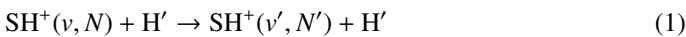
Briefly, the state-average complete active space (SA-CASSCF) method (Werner & Knowles 1985) was employed to calculate the first ⁴A'' together with the two first ²A' and the three first ²A'' electronic states. The obtained state-average orbitals and multireference configurations were then used to calculate both the lowest ⁴A'' and ²A'' states energies with the internally contracted multireference configuration interaction method (ic-MRCI; Werner & Knowles 1988) and the Davidson correction (Davidson 1975). For sulfur and hydrogen atoms, the augmented correlation-consistent quintuple zeta (aug-cc-pV5Z) basis sets were used, and all calculations were made using the MOLPRO suite of programs (Werner et al. 2012). These energies were then fit using the GFIT3C procedure (Aguado & Paniagua 1992; Aguado et al. 1998).

The two PESs exhibit completely different topographies. The ⁴A'' electronic state does not present any minimum out of the van der Waals wells in the asymptotic channels and does not present any barrier to the SH⁺ + H → H₂ + S⁺ reaction. This reaction is exothermic on this surface, and reactive collisions are likely to occur in competition with the inelastic collisions.

On the other hand, the ²A'' state presents a deep insertion HSH well and does not present any barrier either. For this state, in contrast with the previous case, the SH⁺ + H → H₂ + S⁺ reaction is endothermic, and only inelastic collisions can occur (pure or involving H exchange).

2.2. Time-independent and wave packet calculations

During a collision between SH⁺ and H, three processes compete: the inelastic (1), reactive (2), and exchange (3) processes:



where v and N designate the vibrational and rotational levels, respectively, of the molecule (SH⁺ or H₂ when the

reaction occurs). Only collisions with SH⁺ molecules in their ground-vibrational state $v = 0$ are considered in this work. Therefore, the vibrational quantum number v is omitted hereafter.

The spin-orbit couplings between the different H₂S⁺ were ignored and the collisions on the ground quartet and doublet electronic states were studied separately. Because of their different topography, the dynamical calculations were treated differently on the two PESs.

The reaction dynamics on the ⁴A'' state was studied with a time-independent treatment based on hyperspherical coordinates. On this PES, the SH⁺ + H → H₂ + S⁺ collision is a barrierless and exothermic reaction for which it has been shown (Zanchet et al. 2019) that the reactivity is strong ($k > 10^{-10}$ cm³ s⁻¹), even at low temperatures. The competition between all the three processes (inelastic, exchange, and reactivity) is therefore rigorously taken into account. We used the ABC reactive code of Skouteris et al. (2000) to carry out close-coupling calculations of the reactive, inelastic, and exchange cross sections. The cross sections were obtained following the approach described in Tao & Alexander (2007), which was recently used to study the rotational excitation of HeH⁺ (Desrousseaux & Lique 2020) by H.

We computed the cross sections for the first 13 rotational levels of the SH⁺ molecule ($0 < N < 12$) for a collisional energy ranging from 0 to 5000 cm⁻¹ and for all values of the total angular momentum J leading to a nonzero contribution in the cross sections. More details about the scattering calculations can be found in Zanchet et al. (2019).

The ground doublet (²A'') electronic state exhibits a deep well. Therefore time-independent treatment cannot be used, and the dynamics was studied from a quantum wave-packet method using the MAD-WAVE3 program of Zanchet et al. (2009). In this electronic state, the reactive channels are largely endothermic and are not open at the collisional energies considered in this work.

The inelastic and exchange cross sections in the ²A'' state were calculated with the usual partial wave expansion as

$$\sigma_{\alpha, N \rightarrow \alpha', N'}(E_k) = \frac{\pi}{k^2} \frac{1}{2N+1} \sum_{J=0}^{J_{\max}} \sum_{\Omega, \Omega'} (2J+1) \times P_{\alpha v N \Omega \rightarrow \alpha' v' N' \Omega'}^J(E_k), \quad (4)$$

where J is the total angular momentum quantum number, and Ω, Ω' are the projections of the total angular momentum on the reactant and product body-fixed z -axis, respectively. $\alpha = I, \alpha' = I$, or E denotes the arrangement channels, inelastic or exchange. $k^2 = 2\mu_r E_k / \hbar^2$ is the square of the wave vector for a collisional energy E_k , and $P_{\alpha v N \Omega \rightarrow \alpha' v' N' \Omega'}^J(E_k)$ are the transition probabilities, that is, the square of the corresponding S -matrix elements. We computed the cross sections from the $N = 0$ rotational states to the first 13 rotational levels of the SH⁺ molecule ($0 < N' < 12$) for a collisional energy ranging from 0 to 5000 cm⁻¹. Because of the high computational cost of these simulations, they were only performed for $J = 0, 10, 15, 20, 25, 30, 40, 50, \dots, 110$, while for intermediate J values, they were interpolated using a uniform J -shifting approximation as recently used for the OH⁺–H and CH⁺–H collisional systems (Werfelli et al. 2015; Bulut et al. 2015). The convergence analysis and the parameters used in the propagation for each of the two PESs are described in detail in Zanchet et al. (2019).

For the two sets of calculations the corresponding cross sections are summed for the doublet and quartet states

independently because the two rearrangement channels, inelastic and exchange, yield the same products. Finally, the cross sections for each of the two electronic states of quartet (with an electronic spin $S = 3/2$) and doublet (with an electronic spin $S = 1/2$) spin multiplicity were summed with the proper degeneracy factor to give the total collision cross sections as

$$\sigma_{N \rightarrow N'}(E_k) = \frac{2}{3} \sigma_{N \rightarrow N'}^{S=3/2}(E_k) + \frac{1}{3} \sigma_{N \rightarrow N'}^{S=1/2}(E_k). \quad (5)$$

As shown in Zanchet et al. (2019), the magnitude of the excitation cross sections obtained on the doublet states is stronger than that on the quartet states because of the nonreactive character of the collision and of the deep well, which both favor inelastic collisions.

From the total collision cross sections $\sigma_{N \rightarrow N'}(E_k)$, we can obtain the corresponding thermal rate coefficients at temperature T by an average over the collision energy (E_k),

$$k_{N \rightarrow N'}(T) = \left(\frac{8}{\pi \mu k_B^3 T^3} \right)^{\frac{1}{2}} \times \int_0^{\infty} \sigma_{N \rightarrow N'}(E_k) E_k \exp(-E_k/k_B T) dE_k, \quad (6)$$

where k_B is Boltzmann's constant and μ is the reduced mass. The cross-section calculations carried out up to a kinetic energy of 5000 cm^{-1} allowed computing rate coefficients for temperatures ranging from 10 to 1000 K.

In all these calculations, the spin-rotation couplings of SH⁺ were not included, and therefore the present set of rate coefficients cannot be directly used to model interstellar SH⁺ spectra where the fine and hyperfine structure is resolved.

2.3. Infinite-order sudden calculations

In this section, we describe how the state-to-state fine and hyperfine rate coefficients for the SH⁺-H collisional system were computed using infinite-order sudden (IOS) methods (Goldflam et al. 1977; Faure & Lique 2012) using the above $k_{0 \rightarrow N'}(T)$ rate coefficients as “fundamental” rate coefficients (those out of the lowest level)

For SH⁺ in its ground electronic $^3\Sigma^-$ state, the molecular energy levels can be described in the Hund case (b) limit¹. The fine-structure levels are labeled by Nj , where j is the total molecular angular momentum quantum number defined by $j = N + S$. S is the electronic spin. For molecules in a $^3\Sigma^-$ state, $S = 1$. This means that three kinds of levels ($j = N - 1$, $j = N$ and $j = N + 1$) exist, except for the $N = 0$ rotational level, which is a single level.

The hydrogen atom also possesses a nonzero nuclear spin ($I = 1/2$). The coupling between I and j results in a splitting of each level into two hyperfine levels (except for the $N = 1$, $j = 0$ level, which remains only one level). Each hyperfine level is designated by a quantum number F ($F = I + j$) that varies between $|I - j|$ and $I + j$.

Using the IOS approximation, we obtain the rate coefficients among the fine structure levels from the $k_{0 \rightarrow L}(T)$ fundamental rate coefficients with the following formula (e.g.,

Corey & McCourt 1983):

$$k_{Nj \rightarrow N'j'}^{\text{IOS}}(T) = (2N + 1)(2N' + 1)(2j' + 1) \sum_L \begin{pmatrix} N' & N & L \\ 0 & 0 & 0 \end{pmatrix}^2 \left\{ \begin{matrix} N & N' & L \\ j' & j & S \end{matrix} \right\}^2 \times k_{0 \rightarrow L}(T), \quad (7)$$

where the parentheses and braces are the 3- j and 6- j symbols. In the usual IOS approach, $k_{0 \rightarrow L}(T)$ is calculated for each collision angle. Here, however, we used the $k_{0 \rightarrow L}(T)$ rate coefficients of Eq. (6), which are obtained with a more accurate quantum method.

The hyperfine resolved rate coefficients can also be obtained from the fundamental rate coefficients following Faure & Lique (2012),

$$k_{NjF \rightarrow N'j'F'}^{\text{IOS}}(T) = (2N + 1)(2N' + 1)(2j + 1)(2j' + 1) \times (2F' + 1) \sum_L \begin{pmatrix} N' & N & L \\ 0 & 0 & 0 \end{pmatrix}^2 \left\{ \begin{matrix} N & N' & L \\ j' & j & S \end{matrix} \right\}^2 \left\{ \begin{matrix} j & j' & L \\ F' & F & I \end{matrix} \right\}^2 \times k_{0 \rightarrow L}(T). \quad (8)$$

In addition, we note that the fundamental excitation rates $k_{0 \rightarrow L}(T)$ were in practice replaced by the deexcitation fundamental rates using the detailed balance relation,

$$k_{0 \rightarrow L}(T) = (2L + 1)k_{L \rightarrow 0}(T), \quad (9)$$

where

$$k_{L \rightarrow 0}(T) = k_{0 \rightarrow L}(T) \frac{1}{2L + 1} e^{\frac{\varepsilon_L}{k_B T}}. \quad (10)$$

ε_L is the energies of the rotational levels L . This procedure was indeed found to significantly improve the results at low temperatures because of the strong threshold effects.

The fine and hyperfine splittings of the rotational states are of a few cm^{-1} and of a few 0.001 cm^{-1} , respectively, and can be neglected compared to the collision energy at $T > 30 - 50 \text{ K}$ so that our approach is expected to be reasonably accurate for the entire temperature range considered in this work. Lique et al. (2016) have investigated the accuracy of the IOS approach in the case of OH⁺-H collisions. It was shown to be reasonably accurate (within a factor of 2), even at low temperature, so that we can anticipate a similar accuracy for our collisional system. In addition, we note that with the present approach, some fine and hyperfine rate coefficients are strictly zero. This selection rule is explained by the 3- j and 6- j Wigner symbols that vanish for some transitions. In a more accurate approach, these rate coefficients will not be strictly zero, but will generally be weaker than the other rate coefficients.

3. Results

Using the computational method described above, we generated fine and hyperfine resolved rate coefficients for the SH⁺-H collisional system using the doublet and quartet pure rotational rate coefficients in order to provide the astrophysical community with the first set of data for the SH⁺-H collisional system. In all the calculations, we considered all the SH⁺ energy levels with N , $N' \leq 10$, and we included in the calculations all fundamental rate coefficients with $L \leq 12$. The complete set of (de-)excitation rate coefficients is available online from the LAMDA (Schöier et al. 2005) and BASECOL (Dubernet et al. 2013) websites.

¹ For $^3\Sigma^-$ electronic ground-state molecules, the energy levels are usually described in the intermediate coupling scheme (Gordy & Cook 1984; Lique et al. 2005). However, the use of IOS scattering approach implies that the Hund case (b) limit should be used.

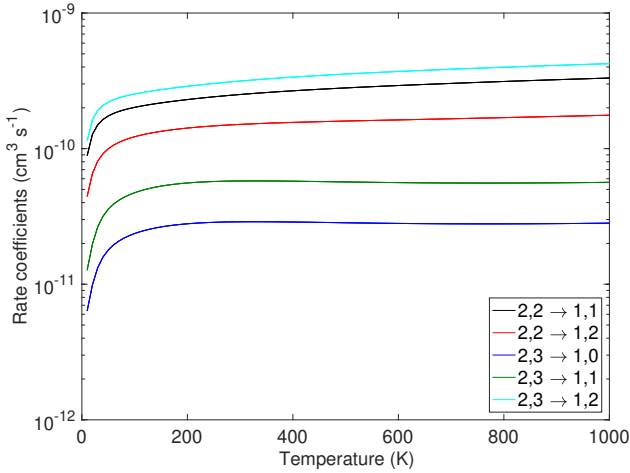


Fig. 1. Temperature variation of the fine structure resolved de-excitation rate coefficients for the SH^+ molecule in collision with H for selected $N = 2, j \rightarrow N' = 1, j'$ transitions.

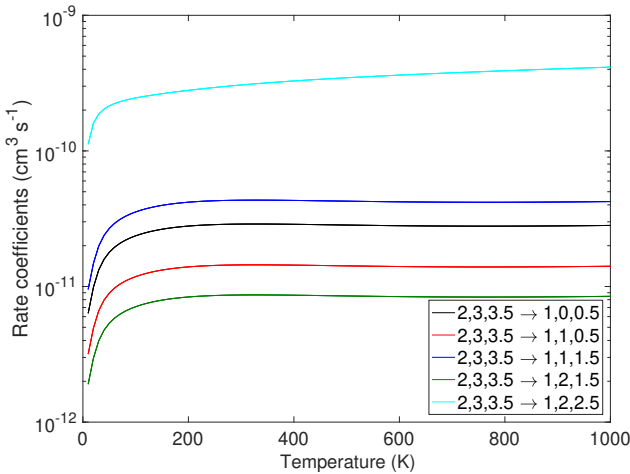


Fig. 2. Temperature variation of the hyperfine structure resolved de-excitation rate coefficients for the SH^+ molecule in collision with H for the $N = 2, j = 3, F = 3.5 \rightarrow N' = 1, j', F'$ transitions.

3.1. Fine- and hyperfine-structure excitation

The thermal dependence of the fine-structure-resolved state-to-state $\text{SH}^+\text{-H}$ rate coefficients is illustrated in Fig. 1 for selected $N = 2, j \rightarrow N' = 1, j'$ transitions.

The temperature variation of the deexcitation rate coefficients is relatively smooth, except at low temperature ($T < 50$ K), where they increase rapidly. The weak temperature dependence of the rate coefficients (except at low temperature) could have been anticipated on the basis of the Langevin theory for ion–neutral interactions.

A strong propensity rule exists for $\Delta j = \Delta N$ transitions. This $\Delta j = \Delta N$ propensity rule was predicted theoretically (Alexander & Dagdigan 1983) and is general for molecules in the $^3\Sigma^-$ electronic state. It was also observed previously for the $\text{O}_2(X^3\Sigma^-)\text{-He}$ (Lique 2010), $\text{NH}(X^3\Sigma^-)\text{-He}$ (Tobola et al. 2011) or $\text{OH}^+\text{-H}$ (Lique et al. 2016) collisions.

Figure 2 presents the temperature variation of the hyperfine-structure-resolved state-to-state $\text{SH}^+\text{-H}$ rate coefficients for selected $N = 2, j = 3, F = 3.5 \rightarrow N' = 1, j', F'$ transitions.

For $\Delta j = \Delta N$ transitions, we have a strong propensity rule in favor of $\Delta j = \Delta F$ hyperfine transitions. This trend

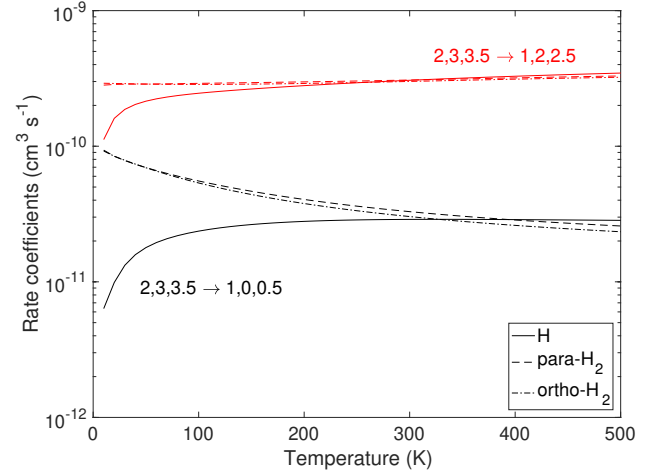


Fig. 3. Comparison between $\text{SH}^+\text{-H}$ and $\text{SH}^+\text{-H}_2$ (both para- and ortho- H_2) rate coefficients for a selected number of hyperfine ($N = 2, j = 3, F = 3.5 \rightarrow N' = 1, j', F'$) transitions.

is the usual trend for open-shell molecules (Alexander 1985; Dumouchel et al. 2012; Kalugina et al. 2012; Lique et al. 2016). For $\Delta j \neq \Delta N$ transitions, it is much more difficult to find a clear propensity rule. The final distribution seems to be governed by two rules: the rate coefficients show propensity in favor of $\Delta j = \Delta F$ transitions, but are also proportional to the degeneracy ($2F' + 1$) of the final hyperfine level, as was found for the $\text{CN}\text{-para-H}_2$ system (Kalugina et al. 2012).

3.2. Comparison with $\text{SH}^+\text{-H}_2$ rate coefficients

We then compared the new $\text{SH}^+\text{-H}$ rate coefficients with those reported recently for the hyperfine excitation of SH^+ by H_2 (Dagdigan 2019). The SH^+ molecule has been observed in media where atomic and molecular hydrogen are significant colliding partners, and this comparison should allow evaluating the effect of the different collisional partners. In Fig. 3 we compare the $\text{SH}^+\text{-H}$ and $\text{SH}^+\text{-H}_2$ (both para- and ortho- H_2) rate coefficients for a selected number of transitions.

In astrophysical applications, when collisional data are not available, it is very common to derive collisional data from collisional rate coefficients calculated for the same molecule in collision with another colliding partner. This approach (Lique et al. 2008) consists of assuming that the excitation cross-sections are similar for the two colliding systems and that the rate coefficients differ only by a scaling factor due to the reduced mass that appears in Eq. (6). Hence, the following scaling relationship can be used:

$$k^{\text{H}} \simeq 1.4 \times k^{\text{H}_2}. \quad (11)$$

At low temperatures, the rate coefficients for collisions with H do not have the highest magnitude, as expected from the scaling relationships. They can even be one order of magnitude weaker. We also note that the differences between the H and H_2 rate coefficients depend on the transitions and on the temperature, which makes it impossible to extrapolate accurate H collisional data from H_2 collisional data, or vice versa. This therefore confirms that it is unrealistic to estimate unknown collisional rate coefficients by simply applying a scaling factor to existing rate coefficients. This result has previously been observed for water (Daniel et al. 2015) and ammonia (Bouhafs et al. 2017). However, when the temperature increases, the agreement improves,

and scaling techniques would lead to a reasonable estimate of the H or H₂ rate coefficients for temperatures above 500 K.

4. Summary and conclusion

The fine and hyperfine excitation of SH⁺ by H were investigated. We obtained fine and hyperfine resolved rate coefficients for transitions involving the lowest levels of SH⁺ for temperatures ranging from 10 to 1000 K. Fine-structure-resolved rate coefficients present strong propensity rules in favor of the $\Delta j = \Delta N$ transition. The $\Delta j = \Delta F$ propensity rule is observed for the hyperfine transitions.

As a molecule that can be observed from ground-based observatories (Müller et al. 2014) in the Milky Way and beyond (Muller et al. 2017), we expect that these new data will significantly help in the accurate interpretation of SH⁺ rotational emission spectra from dense PDRs and massive protostars, enable this molecular ion to act as tracer of the energetics of these regions, and of the first steps of sulfur chemistry.

Acknowledgements. We acknowledge the French-Spanish collaborative project PICS (Ref. PIC2017FR7). F. L. acknowledges financial support from the European Research Council (Consolidator Grant COLLEXISM, Grant agreement 811363), the Institut Universitaire de France and the Programme National “Physique et Chimie du Milieu Interstellaire” (PCMI) of CNRS/INSU with INC/INP co-funded by CEA and CNES. The research leading to these results has received funding from MICIU under grants No. FIS2017-83473-C2 and AYA2017-85111-P. N.B. acknowledges the computing facilities by TUBITAK-TRUBA. This work was performed using HPC resources from GENCI-CINES (Grant A0070411036).

References

- Aguado, A., & Paniagua, M. 1992, *J. Chem. Phys.*, **96**, 1265
 Aguado, A., Tablero, C., & Paniagua, M. 1998, *Comput. Phys. Commun.*, **108**, 259
 Agúndez, M., Goicoechea, J. R., Cernicharo, J., Faure, A., & Roueff, E. 2010, *ApJ*, **713**, 662
 Alexander, M. H. 1985, *Chem. Phys.*, **92**, 337
 Alexander, M. H., & Dagdigian, P. J. 1983, *J. Chem. Phys.*, **79**, 302
 Benz, A. O., Bruderer, S., van Dishoeck, E. F., et al. 2010, *A&A*, **521**, L35
 Benz, A. O., Bruderer, S., van Dishoeck, E. F., et al. 2016, *A&A*, **590**, A105
 Bouhafs, N., Rist, C., Daniel, F., et al. 2017, *MNRAS*, **470**, 2204
 Bulut, N., Lique, F., & Roncero, O. 2015, *J. Phys. Chem., A*, **119**, 12082
 Corey, G. C., & McCourt, F. R. 1983, *J. Phys. Chem.*, **87**, 2723
 Cuadrado, S., Salas, P., Goicoechea, J. R., et al. 2019, *A&A*, **625**, L3
 Dagdigian, P. J. 2019, *MNRAS*, **487**, 3427
 Daniel, F., Faure, A., Dagdigian, P. J., et al. 2015, *MNRAS*, **446**, 2312
 Davidson, E. R. 1975, *J. Comput. Phys.*, **17**, 87
 Desrousseaux, B., & Lique, F. 2020, *J. Chem. Phys.*, **152**, 074303
 Dubernet, M.-L., Alexander, M. H., Ba, Y. A., et al. 2013, *A&A*, **553**, A50
 Dumouchel, F., Klos, J., Tobiola, R., et al. 2012, *J. Chem. Phys.*, **137**, 114306
 Faure, A., & Lique, F. 2012, *MNRAS*, **425**, 740
 Gerin, M., Neufeld, D. A., & Goicoechea, J. R. 2016, *ARA&A*, **54**, 181
 Godard, B., Falgarone, E., Gerin, M., et al. 2012, *A&A*, **540**, A87
 Goicoechea, J. R., Pety, J., Cuadrado, S., et al. 2016, *Nature*, **537**, 207
 Goicoechea, J. R., Cuadrado, S., Pety, J., et al. 2017, *A&A*, **601**, L9
 Goldflam, R., Kouri, D. J., & Green, S. 1977, *J. Chem. Phys.*, **67**, 5661
 Gordy, W., & Cook, R. L. 1984, *Microwave Molecular Spectra* (Wileys and sons)
 Hamilton, J. R., Faure, A., & Tennyson, J. 2018, *MNRAS*, **476**, 2931
 Kalugina, Y., Lique, F., & Klos, J. 2012, *MNRAS*, **422**, 812
 Lique, F. 2010, *J. Chem. Phys.*, **132**, 044311
 Lique, F., Tobiola, R., Klos, J., et al. 2008, *A&A*, **478**, 567
 Lique, F., Bulut, N., & Roncero, O. 2016, *MNRAS*, **461**, 4477
 Lique, F., Spielfiedel, A., Dubernet, M. L., & Feautrier, N. 2005, *J. Chem. Phys.*, **123**, 134316
 Menten, K. M., Wyrowski, F., Belloche, A., et al. 2011, *A&A*, **525**, A77
 Müller, H. S. P., Goicoechea, J. R., Cernicharo, J., et al. 2014, *A&A*, **569**, L5
 Muller, S., Müller, H. S. P., Black, J. H., et al. 2017, *A&A*, **606**, A109
 Nagy, Z., Van der Tak, F. F. S., Ossenkopf, V., et al. 2013, *A&A*, **550**, A96
 Roueff, E., & Lique, F. 2013, *Chem. Rev.*, **113**, 8906
 Schöier, F. L., van der Tak, F. F. S., van Dishoeck, E. F., & Black, J. H. 2005, *A&A*, **432**, 369
 Skouteris, D., Castillo, J. F., & Manolopoulos, D. E. 2000, *Comput. Phys. Commun.*, **133**, 128
 Tao, L., & Alexander, M. H. 2007, *J. Chem. Phys.*, **127**, 114301
 Tobiola, R., Dumouchel, F., Klos, J., & Lique, F. 2011, *J. Chem. Phys.*, **134**, 024305
 Werfelli, G., Halvick, P., Honvault, P., Kerkeni, B., & Stoecklin, T. 2015, *J. Chem. Phys.*, **143**, 114304
 Werner, H.-J., & Knowles, P. J. 1985, *J. Chem. Phys.*, **82**, 5053
 Werner, H.-J., & Knowles, P. J. 1988, *J. Chem. Phys.*, **89**, 5803
 Werner, H.-J., Knowles, P. J., Knizia, G., Manby, F. R., & Schütz, M. 2012, *WIREs Comput. Mol. Sci.*, **2**, 242
 Zanchet, A., Agúndez, M., Herrero, V. J., Aguado, A., & Roncero, O. 2013, *AJ*, **146**, 125
 Zanchet, A., Roncero, O., González-Lezana, T., et al. 2009, *J. Phys. Chem. A*, **113**, 14488
 Zanchet, A., Lique, F., Roncero, O., Goicoechea, J. R., & Bulut, N. 2019, *A&A*, **626**, A103